*catalysts*

MDPI

*Article*

# Steel Slag as a Highly Efficient Catalyst for the Hydrodeoxygenation of Fatty Acids: From a Waste to a Precious Material for Renewable Fuels Production

**Stefano Savino [1], Elena Ghedini [2,*], Tommaso Castiglia [2], Rosella Attrotto [3], Giuseppe Guglielmo [3], Francesco Taddeo [4], Michela Signoretto [5], Lucia D'Accolti [1,2,†] and Angelo Nacci [1,2,†]**

[1] Institute of Chemistry of Organometallic Compounds-National Research Council-CNR, SS Bari, Via Orabona 4, 70125 Bari, Italy; stefano.savino@iccom.cnr.it (S.S.); lucia.daccolti@uniba.it (L.D.); angelo.nacci@uniba.it (A.N.)
[2] Chemistry Department, University of Bari Aldo Moro, 70125 Bari, Italy; t.castiglia@phd.uniba.it
[3] Research and Development, Acciaierie d'Italia S.p.A., SS Appia km 648, 74123 Taranto, Italy; rosella.attrotto@adiinas.com (R.A.); giuseppe.guglielmo@adiinas.com (G.G.)
[4] Department of Chemical Science, University of Napoli Federico II, Via Cintia, 80126 Napoli, Italy; francesco.taddeo@unina.it
[5] Department of Molecular Sciences and Nanosystems, Ca' Foscari University of Venice, INSTM RU of Venice, via Torino 155, 30172 Venice, Italy; miky@unive.it
* Correspondence: elena.ghedini@uniba.it
† These authors contributed equally to this work.

**Abstract**

With no precedent in the literature, steel slag, an inexpensive and plentiful by-product of the steel industry, was discovered to be a highly selective and active catalyst for the hydrodeoxygenation (HDO) of triglycerides and fatty acids. This material, which is not always recyclable, proved to perform in the virgin state (without any chemical pretreatment), actually fostering the conversion, via a hydrothermal reaction, of palmitic and stearic acids into the corresponding (C16 and C18) alkanes with selectivity above 90%. In addition, by moving to a more complex system such as soybean oil, a complete conversion and the possibility of recycling the catalyst were maintained. Catalytic material, which came from an Italian steel industry (Acciaierie d'Italia), was characterized by XRF, XRD, $N_2$ physisorption analyses, TPR, and TPD techniques. Catalytic performance was successfully correlated with the characterization results, and mechanistic proofs were provided on the catalytic role played by the several iron species present in the slag. The results reported in this work represent a significant contribution to the large-scale production of green diesel and, thanks to the possibility of using a catalyst based on steel slag in HDO processes, open the way to decarbonization and climate neutrality processes.

**Keywords:** steel slag; green diesel; HDO; catalysis; green chemistry; circular economy

Check for updates

Academic Editors: Anjie Wang and Ivan V. Kozhevnikov

Received: 8 January 2026
Revised: 11 February 2026
Accepted: 17 February 2026
Published: 24 February 2026

**Copyright:** © 2026 by the authors. Licensee MDPI, Basel, Switzerland. This article is an open access article distributed under the terms and conditions of the Creative Commons Attribution (CC BY) license.

## 1. Introduction

The worldwide transition toward sustainable energy and the need for reducing greenhouse gas emissions (GHG) have driven substantial research into renewable fuels [1,2]. Among numerous biomass feedstocks, fatty acids (FAs) have drawn attention due to their vast availability and potential for conversion into high-energy hydrocarbons [3]. One of the most promising methods for upgrading FAs is hydrodeoxygenation (HDO), a catalytic process that removes oxygen from long carbon chains of carboxylic acid functionalities, converting these compounds into alkanes, alkenes, and other hydrocarbons,

thus enhancing their energy density while simultaneously improving their stability and combustion properties.

This strategy results in the production of hydrocarbons suitable for use as jet fuel or renewable diesel [4]. The latter, known as green diesel, is the biofuel possessing the same composition ($C_{15}$-$C_{18}$) of fossil diesel, but showing properties that make it a valuable green alternative (e.g., higher cetane number, lower sulphur content, higher energy density, etc.). Such features also allow it to overcome the limitations of 1st generation biodiesel (the so-called FAMEs), which typically include higher oxygen content, pour point and viscosity, and low compatibility with conventional engines [5,6].

The HDO reaction of fatty acids normally requires harsh conditions ($P_{H2}$ in the range of 4–12 MPa and T of 200–450 °C) and either noble or non-noble metal catalysts, preferentially anchored on supports (silica, alumina, zeolites, etc.) and assembled in sulfide, bimetallic, or alloy form [7]. The incorporation of acidic or basic sites can further influence product distribution, enabling better control over the reaction pathway. To date, the high cost of noble metals (Pd, Pt, Ru [8–11]), which limits their large-scale application, as well as the sulfur leaching observed with sulfide catalysts, which leads to contamination of the alkane products, are serious problems to circumvent, and the rational design of a highly active and stable catalyst remains a key challenge.

Consequently, non-noble metals (Ni, Co, Cu, Mo, Fe, etc. [6]) have recently received greater attention in mediating the HDO reaction of FAs. Among them, nickel-based materials proved to be the best-performing catalysts, with more than fifteen reports only in the last five years [12,13].

In this context, the use of steel slag is particularly intriguing, an abundant and cheap by-product of the steel industry that seems to be an ideal candidate for large-scale applications (8.5 Mt produced in Europe in 2023 [14,15]). Even if up to 80% of the slags are already recycled, they are only used as inert materials, particularly in the civil sector [14,16]. However, by virtue of its composition, which is rich in metals, a better option to valorize this material is to turn it into an efficient and recyclable catalyst [17].

Our prior investigations have already demonstrated that steel slag displays good catalytic characteristics in the energy sector, facilitating the $CO_2$ photo- and thermo-reduction to solar fuels [18,19] and the transesterification of triglycerides [20] to generate FAMEs. In this regard, we hypothesized that this industrial waste may be utilized as a valuable HDO catalyst, expanding the material's spectrum of uses to the catalytic field where it has never been employed.

We report herein an unprecedented catalytic ability displayed by steel slag in the hydrodeoxygenation of fatty acids (palmitic and stearic) and soybean oil to produce the corresponding alkanes (hexadecane and octadecane). Notably, the material is efficient and highly selective for HDO without any chemical or thermal pretreatment, thereby enabling a high circularity rate. Such features, together with the large volume of unrecycled steel slag produced yearly (about 1.1 Mton in 2023) [14], suggest a high feasibility for the large-scale extension of this protocol.

## 2. Results

### *2.1. Steel Slag Selection*

Slags play a fundamental role in the liquid steel production process as they allow the removal of unwanted components such as $SiO_2$, $Al_2O_3$, sulfur, and phosphorous. The slag material used in the present study was obtained from an Italian integral cycle steel plant (Acciaierie d'Italia). Besides blast furnace (BF) slag, other types of residues are produced during the successive steps of the steelmaking process. All these materials are classified as

intermediate, waste or by-products depending on their composition and destination after production, as shown in Table 1.

**Table 1.** Typical slag composition of integrated steelmaking plants [(a)].

| Slag Matrix [(b)] | $SiO_2$ | $Al_2O_3$ | CaO | MgO | TiO | $Fe_2O_3$ [(c)] | $P_2O_5$ | MnO | C | S | Classification [(d)] | Destination [(d)] |
|---|---|---|---|---|---|---|---|---|---|---|---|---|
| Blast furnace | 30–35 | 10–15 | 40–45 | 5–10 | <1 | <1 | ~0 | ~0 | ~0 | <1 | 100% by-product | Cement, concrete, road construction |
| Secondary | 5–10 | 35–40 | 35–40 | 5–10 | <1 | 0–5 | ~0 | 0–5 | ~0 | 0.1 | >85% by-product | Most for road construction (by-product) |
| Converter (BOF) | 10–15 | 5–10 | 45–50 | 5–10 | <1 | 20–25 | <2 | 0–5 | ~0 | ~0 | <15% waste | Landfilled or for filling quarries (waste) |

[(a)] According to ADI analyses and [12]. [(b)] Slag origin and its average weight% compositions. [(c)] Sum of all iron oxides present, here reported as $Fe_2O_3$. [(d)] Data from [14].

Blast furnace slag (BF), converter slag (BOF) and slag from secondary treatment are generally considered to be residues or by-products with a high intrinsic value, containing recoverable elements for different sectors. Despite this, steel slag is not always easily recyclable, as mentioned above.

With the ambition of transforming steel slag into a precious catalyst for energy production, we selected BOF slag for this study. The rationale behind this choice was (i) the abundance of this material among the steel slags produced in Europe annually (60%); (ii) the noticeable percentage that is landfilled as waste (about 15% corresponding to 1 Mt per year [14]); (iii) the remarkable iron oxides content (20–25%), which we speculate to be the HDO active species; and finally (iv) the absence of dangerous elements that can be present in other materials, such as EAF slag, due to the use of scraps [21].

In order to evaluate the catalytic performance of BOF slag, two main grain sizes were selected after the grinding and sieving of the pristine material: sizes < 1600 μm (labeled as SLAG-1600) and sizes in the range 90–210 μm (labeled as SLAG-90). Both slag samples were used throughout all the experiments without any further treatment (see Materials and Methods section).

The purpose of using two different particle sizes, rather than just the largest, lies in the influence of particle size on catalyst activity and surface area. Smaller particles generally offer a larger surface area, which can increase the availability of active sites for the catalytic reaction. On the other hand, larger particles can exhibit different diffusion properties and provide a more stable catalytic environment under certain conditions. By testing both particle sizes, we aimed to evaluate how variations in surface area and particle size distribution affect the selectivity, activity, and overall efficiency of the hydrodeoxygenation process. Furthermore, using both particle sizes allowed for a more in-depth investigation of the material's performance under real-world conditions, where particle size distribution can vary due to processing or handling.

### *2.2. Catalyst Characterization*

The slag fractions were thoroughly characterized by means of XRD, XRF, and SEM-EDX techniques together with physiochemical analyses (adsorption/desorption isotherms, BET, BJH, TPD and TPR).

#### 2.2.1. Mineralogical Analyses

X-ray diffraction (XRD) analyses provided information about the crystalline phases present in the slag fractions (Figures S1 and S2). The data in Table 2 show the weight distributions of such phases that mainly arise from calcium, aluminum and iron oxides, with small amounts of metallic Fe, MgO and $MnO_2$. The distribution appears to be dependent on the grain size as it varies from SLAG-1600 to SLAG-90.

**Table 2.** XRD analyses.

| Phases | Weight Distribution (%) | |
|---|---|---|
| | **SLAG-90 (90–210 μm)** | **SLAG-1600 (<1600 μm)** |
| Larnite, $Ca_2SiO_4$ | 65.1 | 39.6 |
| Gehlenite, $Ca_2Al(SiAl)O_7$ | 0 | 10.2 |
| Wustite, FeO | 6.2 | 10.7 |
| Hematite, $Fe_2O_3$ | 0 | 12.1 |
| Magnetite, $Fe_3O_4$ | 5.8 | 4.2 |
| Srebrodolskite, $Ca_2Fe_2O_5$ | 9.7 | 14.7 |
| Periclase, MgO | 0 | 6.1 |
| Metallic, Fe | 5.1 | 2.4 |
| Ramsdellite, $MnO_2$ | 2.2 | 0 |

The chemical composition (elements and oxides) of the slag materials was studied by means of X-ray fluorescence analyses (Table 3). The results highlighted the distribution of elements and oxides between the two fractions under study, confirming a substantial homogeneity for several components, with narrow ranges for most of the elements and oxides, except for CaO and $Fe_2O_3$.

**Table 3.** XRF analyses *.

| Element/Oxide | Weight Distribution (%) | |
|---|---|---|
| | **SLAG-90 (90–210 μm)** | **SLAG-1600 (<1600 μm)** |
| CaO | 40.36 | 34.17 |
| $SiO_2$ | 13.56 | 12.34 |
| $P_2O_5$ | 0.53 | 0.58 |
| S | 0.05 | 0.15 |
| $Al_2O_3$ | 3.18 | 5.57 |
| MgO | 7.59 | 7.37 |
| $Fe_2O_3$ | 22.65 | 31.75 |
| $TiO_2$ | 0.44 | 0.46 |
| MnO | 1.15 | 1.47 |
| L.O.I. [(a)] | 10.33 | 6.14 |

[(a)] Loss of ignition. * Instrumental error: ±0.02.

SEM analyses were carried out to gain information about the morphology of the two BOF slag fractions (Figure 1).

The elemental surface composition of the catalyst material was determined via EDX (Figures S3–S6) by mapping different spots at different magnifications (100 μm and 25 μm) for both granulometries. In addition, morphologically, the two slag fractions exhibited no significant differences aside from their distinct granulometry. However, EDX analysis revealed that the iron content on the surface was slightly higher in the case of SLAG-90 (Table 4).

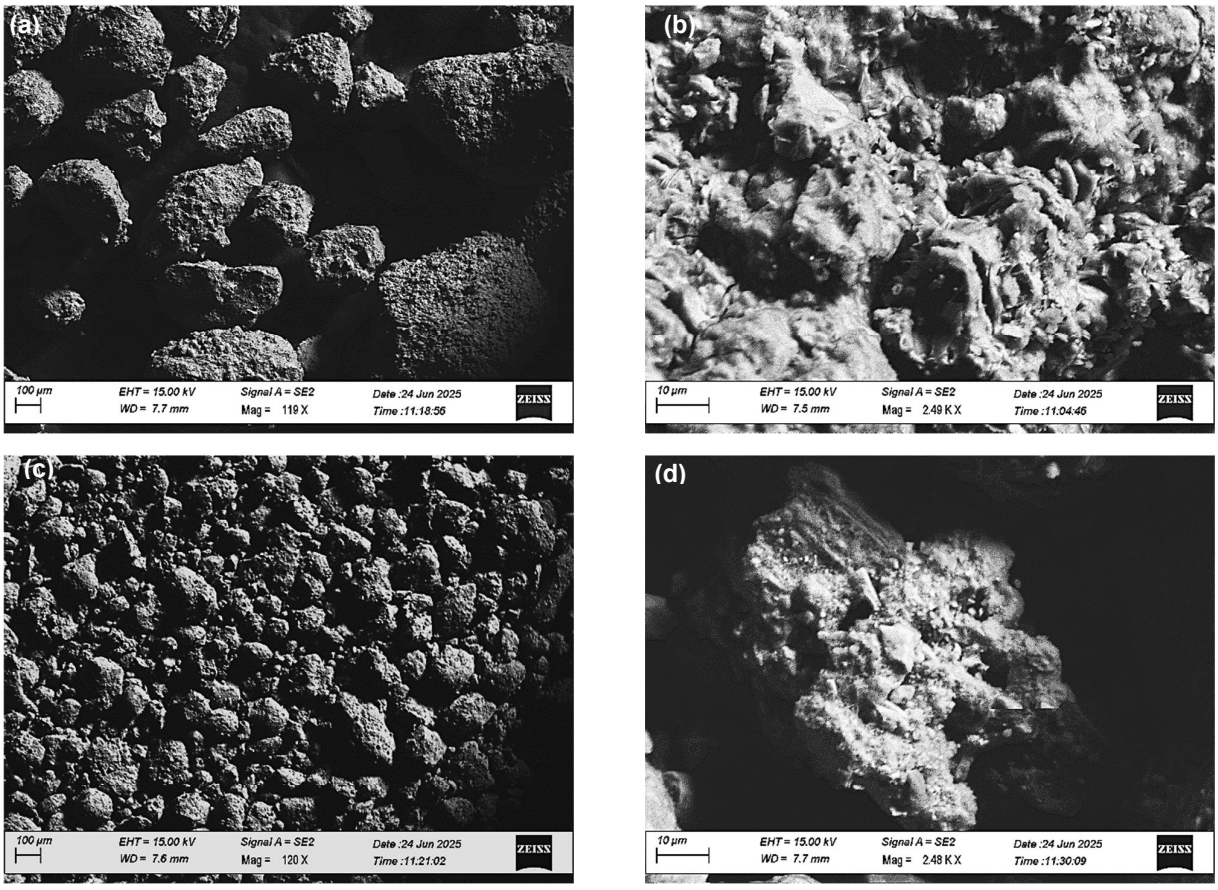



**Figure 1.** SEM images of SLAG-1600: (**a**) overview image at 100 µm, (**b**) 10 µm expanded view; SLAG-90: (**c**) overview image at 100 µm, (**d**) 10 µm expanded view.

**Table 4.** Slag EDX at different magnifications.

| Element | Distribution (%) | | | |
|---|---|---|---|---|
| | SLAG-90 | | SLAG-1600 | |
| | 100 µm | 25 µm | 100 µm | 25 µm |
| O | 57.13 | 56.17 | 56.99 | 53.10 |
| Mg | 0.92 | 0.65 | 2.09 | 2.20 |
| Al | 1.34 | 1.00 | 0.00 | 1.31 |
| Si | 6.39 | 5.04 | 6.20 | 5.67 |
| Ca | 31.43 | 32.85 | 32.51 | 34.40 |
| Fe | 2.80 | 4.29 | 2.22 | 3.33 |
| Total | 100.00 | 100.00 | 100.00 | 100.00 |

The results confirmed the XRF analyses and showed a substantial homogeneity for several elements on the slag surface independent of the grain size.

However, all these data required more specific physiochemical analyses to determine the abundance of active sites on the surfaces of several fractions.

### 2.2.2. Physiochemical Analyses

To gain information on the surface features of slag, $N_2$ physisorption analyses were conducted (Figure 2). The adsorption/desorption isotherms of SLAG-90 (Figure 2a,b) and

SLAG-1600 (Figure 2c,d) were very similar, in accordance with the IUPAC nomenclature, revealing a type III isotherm characterized by a convex shape, which is typical of weak interactions with the gas phase. Additionally, the isotherm exhibited an H3 hysteresis loop, commonly associated with the presence of interstitial pores formed by particle aggregates. Overall, the materials can be classified as mesoporous (2–50 nm), as demonstrated in Figure 2b, with a heterogeneous pore network characterized by a broad pore size distribution with large pores. Finally, the $S_{BET}$ surface area values were very low in the case of both samples: 6 $m^2$ $g^{-1}$ for the SLAG-90 and 10 $m^2$ $g^{-1}$ for SLAG-1600. These results suggest that the different mean particle size of the samples does not demonstrate a significant change in the porous structure of the materials.

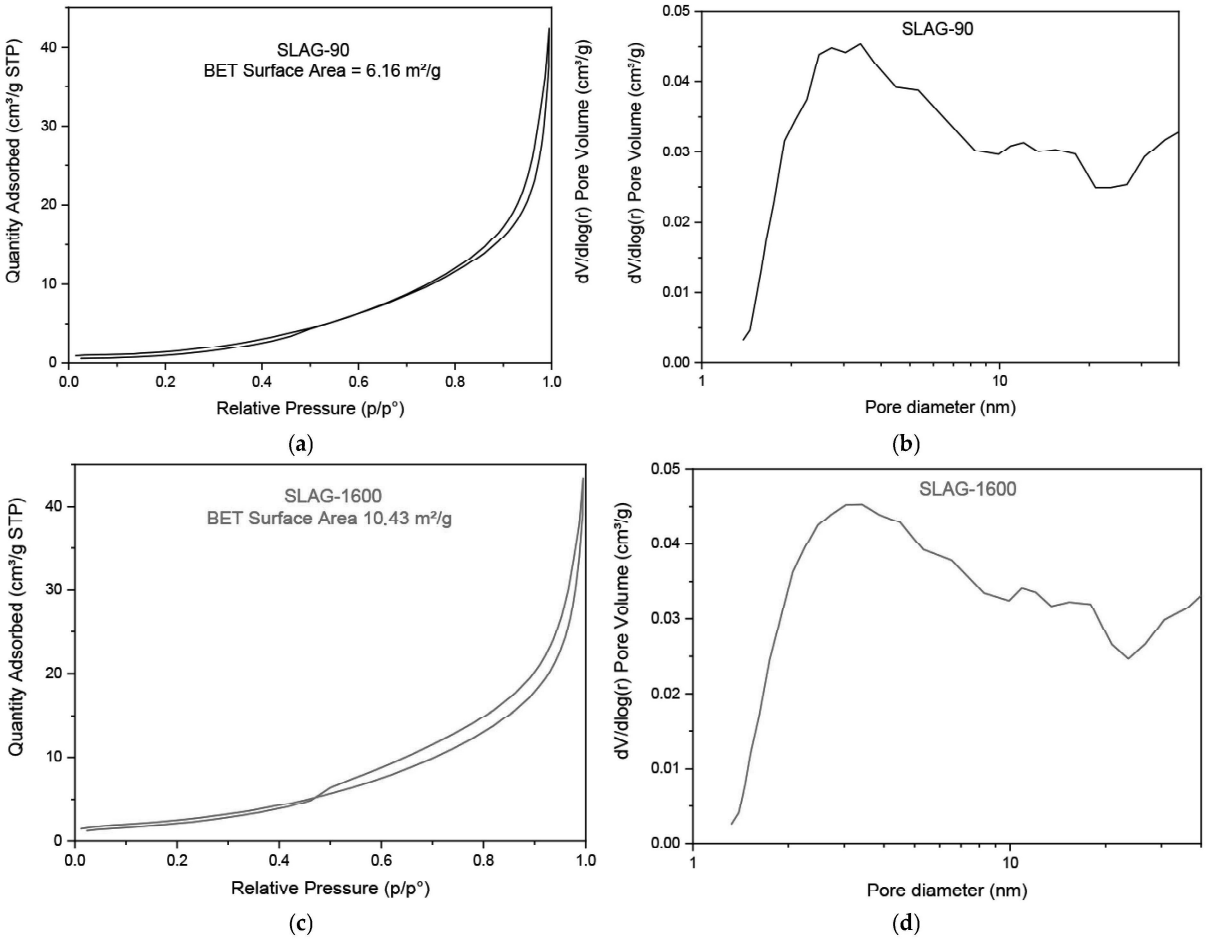



**Figure 2.** Adsorption–desorption isotherms at 100 °C of (**a**,**b**) SLAG-90 and (**c**,**d**) SLAG-1600 samples. Instrument error: ±0.03.

The $H_2$-TPR profiles of the SLAGs are shown in Figure 3a. For both samples, two main bands from 400 to 900 °C can be observed. The peaks can be attributed to the reduction of different iron species. According to previous reports [22], the reduction of $Fe^{3+}$ to $Fe^{2+}$ in isolated ions, oligomeric clusters or nanoparticles is responsible for TPR peaks below 500 °C, whereas the reduction of $Fe^{2+}$ to $Fe^0$ in oligomeric clusters or nanoparticles is ascribed to peaks between 500 and 900 °C. The two reduction profiles are practically overlapped to indicate that, regardless of the sieving, the redox behavior of the samples remains unchanged.

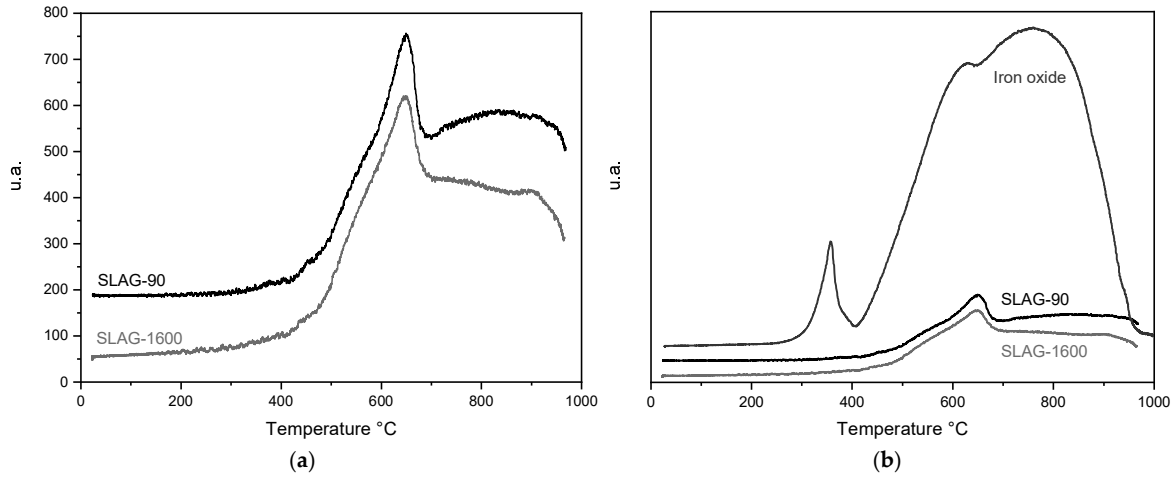



**Figure 3.** $H_2$-TPR profiles for (**a**) SLAG-90 and SLAG-1600, (**b**) iron oxides, SLAG-90 and SLAG-1600.

Figure 3b shows the TPR profile of iron(III) oxide A-$Fe_2O_3$ (hematite) compared with the catalyst profiles previously shown.

The typical TPR-$H_2$ profile of the iron oxide consists of two fairly well separated reduction peaks; the smaller low-temperature peak (300 °C) of the TPR curve, reflects the first stage of the reduction of hematite to magnetite ($\alpha$-$Fe_2O_3 \rightarrow Fe_3O_4$), and the second broad and much larger high-temperature peak (T > 400 °C) represents the reduction of magnetite to metallic iron ($Fe_3O_4 \rightarrow Fe$) [23]. In the TPR profile of both SLAGs, exactly the same higher temperature reduction band is present as in the iron oxide TPR curve. This confirms that the two main crystalline phases of iron oxide present in SLAGs are magnetite and wüstite, which is in accordance with XRD results.

Since the HDO reaction is strongly influenced by the acidity and basicity of the catalysts, measurements of $CO_2$ and ammonia TPDs were performed on the SLAGs to acquire information on the quantity and strength of the surface acid and base sites. The position and area of the desorption peak of the samples determined by $CO_2$-TPD or ammonia-TPD measurements are indicative of the basic and acidic strength and the number of base and acid sites, respectively [24].

As shown in Figure 4a, all samples give two well-defined $CO_2$ desorption bands, which are related to the presence of basic sites with different strengths. The low-temperature desorption peak (<500 °C), with maximum desorption at 450 °C, is due to chemisorption of $CO_2$ on basic sites of medium strength. The $CO_2$ desorption peak at around 600–800 °C reflects, instead, the presence of strong basic sites on the slag surface. A quantitative calculation based on the $CO_2$-TPD and nitrogen physisorption measurements indicates that the surface density of basic sites, defined as the number of moles of $CO_2$ adsorbed per surface area of solids, is almost the same in both analyzed SLAGs (~85 μmol/$m^2$). The TPD profiles of ammonia are shown in Figure 4b. In the case of SLAG-1600, there is only one well-defined peak centered at 300 °C that can be associated with medium-strength acid sites.

The lower-grain-size sample (SLAG-90) shows, on the other hand, two bands. The first, at the lower temperature (120 °C), is correlated to interaction with weak surface acid sites, and the second, at 300 °C, is associated, as in the case of the previous sample, with the presence of acidic sites of medium strength. The amount of chemisorbed ammonia is different in the two samples: 100 μmol/$m^2$ for SLAG-90 compared to 80 μmol/$m^2$ for SLAG-1600. These experimental data indicate not only the presence of acid sites of different strength on the two samples but also a higher overall surface acidity in the SLAG with the lower grain size (SLAG-90). This TPD response can be associated with the surface metal

composition highlighted by the SEM-EDX analyses. Indeed, in the SLAG-90 sample, the iron content seems slightly higher than in the SLAG-1600 sample, justifying the different balance and amount of acid sites revealed by TPD measurements.

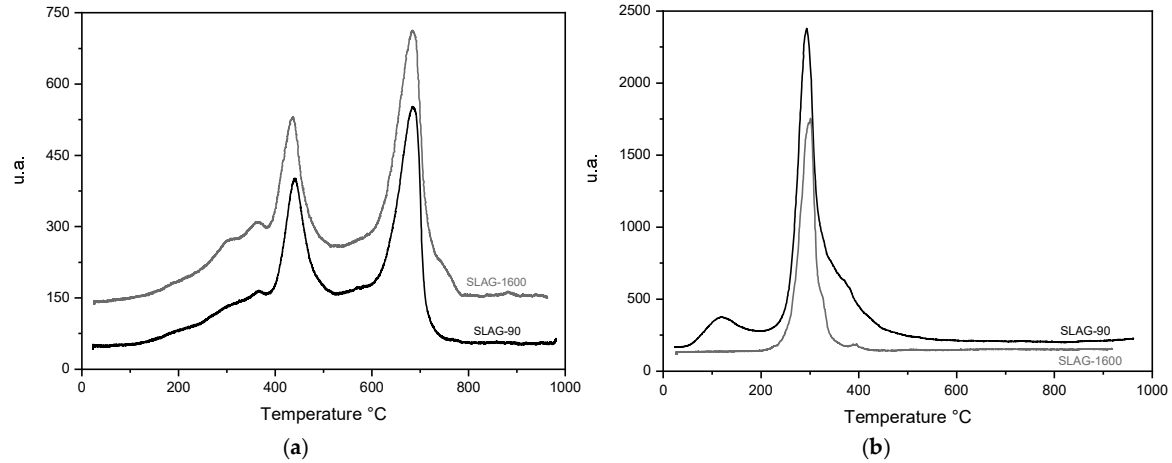



**Figure 4.** (**a**) $CO_2$-TPD and (**b**) ammonia-TPD profiles for slags.

### *2.3. Catalytic Test*

The literature was consulted in selecting the hydrodeoxygenation conditions [25]. Using the pristine slag as a catalyst (sizes < 1600 μm), the experimental set-up was calibrated to handle 100–500 mg of fatty acids under a hydrogen pressure of 15 bar. From the preliminary experiments conducted on two representative substrates, namely palmitic (PA) and stearic acid (SA), encouraging results emerged, attested by a complete and highly selective conversion (>90%) of these model fatty acids into the corresponding HDO products, hexadecane (C16) and octadecane (C18), as is evident in the GC-chromatograms displayed in Figure 5 [2].

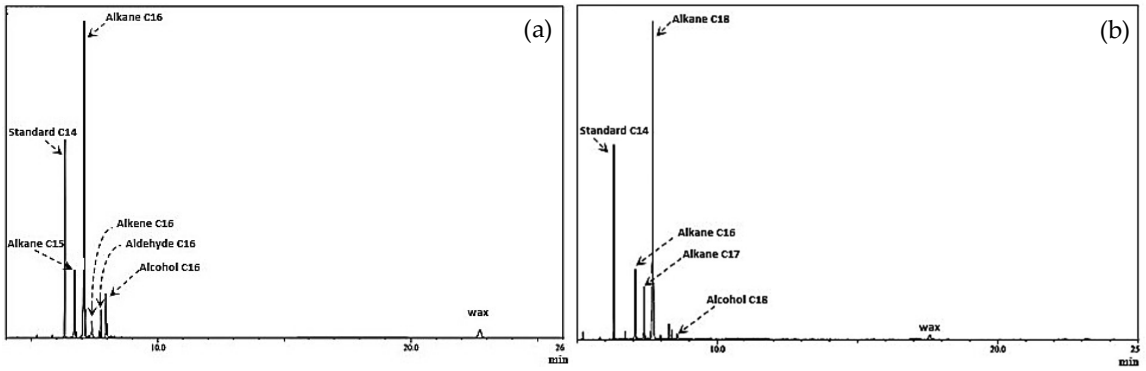
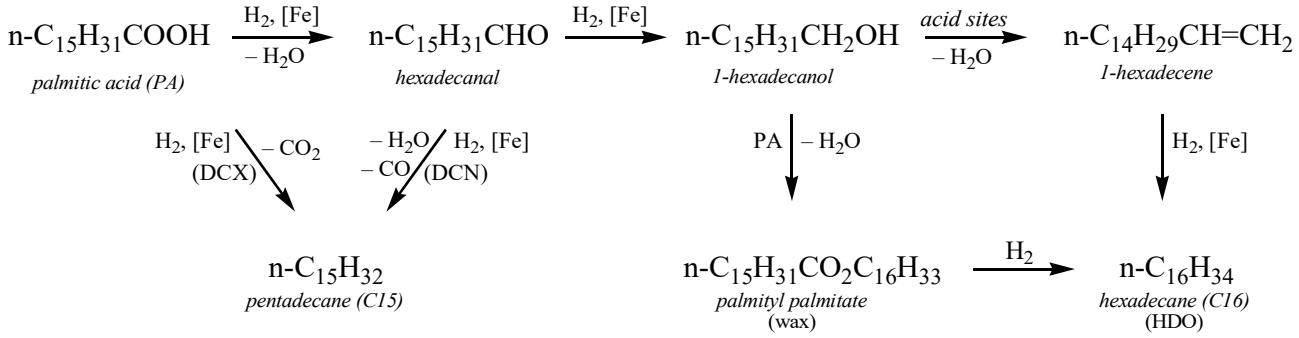



**Figure 5.** Representative GC chromatograms of HDO reaction mixture for palmitic acid (**a**) and stearic acid (**b**). HDO conditions: fatty acid 100 mg, slag catalyst 300 mg, 5 mL of hexane, $P_{H2}$ = 15 bar, T = 260 °C, time = 10 h. Tetradecane was used as an internal standard.

Besides the expected alkanes, small amounts of the reaction intermediates, namely aldehydes, alcohols, alkenes, and esters (waxes), were observed, together with the decarbonylation (DCN) and decarboxylation (DCX) side-products (C15 and C17).

All of them were formed according to the reaction pathways listed in Scheme 1, where iron oxides are assumed to be the catalytically active species (see Section 3.1) [20,26]. These results were obtained with both palmitic and stearic acids, thus confirming the slag as a superior catalyst capable of achieving very high selectivity in the HDO of fatty acids.




**Scheme 1.** Reaction pathways in HDO of fatty acids.

The successive catalytic experiments were carried out with palmitic acid as the substrate. Firstly, the influence of the substrate/slag ratio was surveyed using the largest-grained slag powder (SLAG-1600). As can be seen in Figure 6a, the expected decreased catalytic activity (caused by the large granule sizes) was used to increase the impact of this parameter. With a substrate/slag ratio of 5:3, a very low conversion was observed, suggesting that the massive amounts of PA substrate adsorbed on the catalyst surface had an inhibitory effect. Conversions increased when the ratio was reversed in favor of the slag, eventually reaching completeness with a 1:3 ratio. The blank experiment, conducted without the slag, confirmed that this material is truly a catalyst for the process.

Notably, the data in Figure 6a clearly show that steel slag behaves as a precious catalyst, yielding the hydrodeoxygenation product (C16) with a selectivity of 90%, a truly astonishing result considering that this material is made from a non-pretreated, inhomogeneous waste powder possessing large grain sizes.

Next, due to the low TONs (turnover numbers) exhibited by the largest grains (SLAG-1600), the influence of particle dimension was examined by comparison with the smaller slag particles. Adopting a substrate:slag ratio of 5:3, conversion remarkably increased with the decrease in grain sizes, passing from 10% (SLAG-1600) to 90% (SLAG-90) (Figure 6b). The difference in productivity is associated with the different surface properties exhibited by the two catalysts. In the case of the sample with the lower grain size, the higher concentration of surface iron ensured the availability of a greater number of active metal sites and a catalytic surface with an optimal synergy of low- and medium-strength acid sites, as highlighted by ammonia-TPD experiments (Figure 4b).

The HDO reaction was likewise predictably impacted by temperature. To magnify the influence of such a parameter, an even higher substrate/slag ratio of 5:1 (*wt*/*wt*), together with the smaller slag size (SLAG-90), were adopted, monitoring a large temperature range (260–340 °C). Due to the growth of undesirable cracking products, heating at temperatures higher than 340 °C was avoided. Expectedly, the temperature increase enhanced the slag performance in a sensible manner, enabling a 60% conversion rate without decreasing selectivity toward HDO products (Figure 6c).

Solvent and reaction time were adjusted by means of the targeted experiments listed in Figure 6d. Hydrocarbon solvents were found to be the best reaction media. Among them, heptane offered the best performance, achieving the maximum conversion and limiting the cracking by-products.

Finally, the hydrogen pressure effect was investigated in the range of 15–30 bar. The lowest temperature in the range (260 °C) was adopted to magnify the effect. The results are shown in Figure 6e. At lower pressure, little conversions were observed, accompanied by high selectivity toward an HDO product. With the increase in $H_2$ pressure, a corresponding increase in fatty acid conversion was observed, but at the same time, the selectivity

gradually decreased due to the formation of cracking by-products. Therefore, 15 bar was selected as the optimal pressure for the successive experiments.

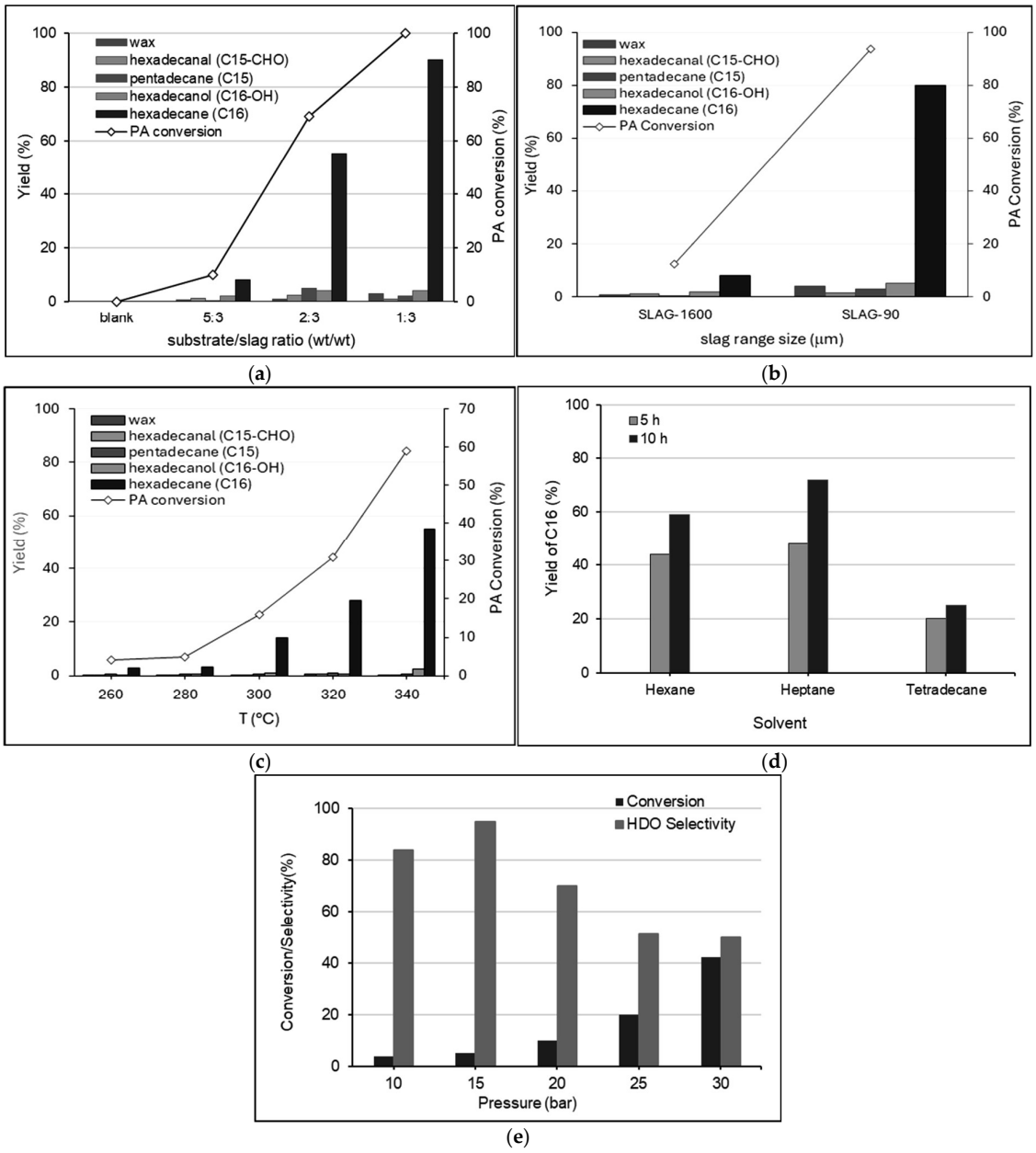



**Figure 6.** Studies of factors affecting Sthe slag-catalyzed HDO reaction. (**a**) Influence of the substrate/slag ratio (*wt*/*wt*): substrate (PA) 100–500 mg, SLAG-1600 300 mg, solvent (hexane) 5 mL, $P_{H2}$ = 15 bar, T = 260 °C, time = 10 h. (**b**) Influence of the slag particle sizes: substrate (PA) 500 mg; slag catalyst 300 mg, solvent (hexane) 10 mL, $P_{H2}$ = 15 bar, T = 260 °C, time = 10 h. (**c**) Temperature dependence: substrate (PA) 500 mg, SLAG-90 100 mg (5:1 *wt*/*wt*), solvent (hexane) 10 mL, $P_{H2}$ = 15 bar, time = 10 h. (**d**) Solvent and time effect: substrate (PA) 500 mg, SLAG-90 100 mg (5:1 *wt*/*wt*), solvent 10 mL, $P_{H2}$ = 15 bar, T = 340 °C, and time = 10 h. In the case of tetradecane, conspicuous amounts of cracking products were found. (**e**) Pressure dependence: substrate (PA) 500 mg, SLAG-90 100 mg, solvent (hexane) 10 mL, T = 260 °C, time = 5 h.

A final optimization test was carried out to incorporate the optimal energetic conditions and accomplish quantitative conversion after these crucial parameters were methodically investigated. A yield of around 100% of the hydrodeoxygenation product (C16) was successfully obtained using a substrate/slag ratio of 2:3, the finest slag powder (SLAG-90),

a temperature of 260 °C, heptane as the solvent, and a hydrogen pressure of 15 bar. This outcome validates the improved protocol's great efficacy.

## 3. Discussion

### *3.1. Mechanistic Insight*

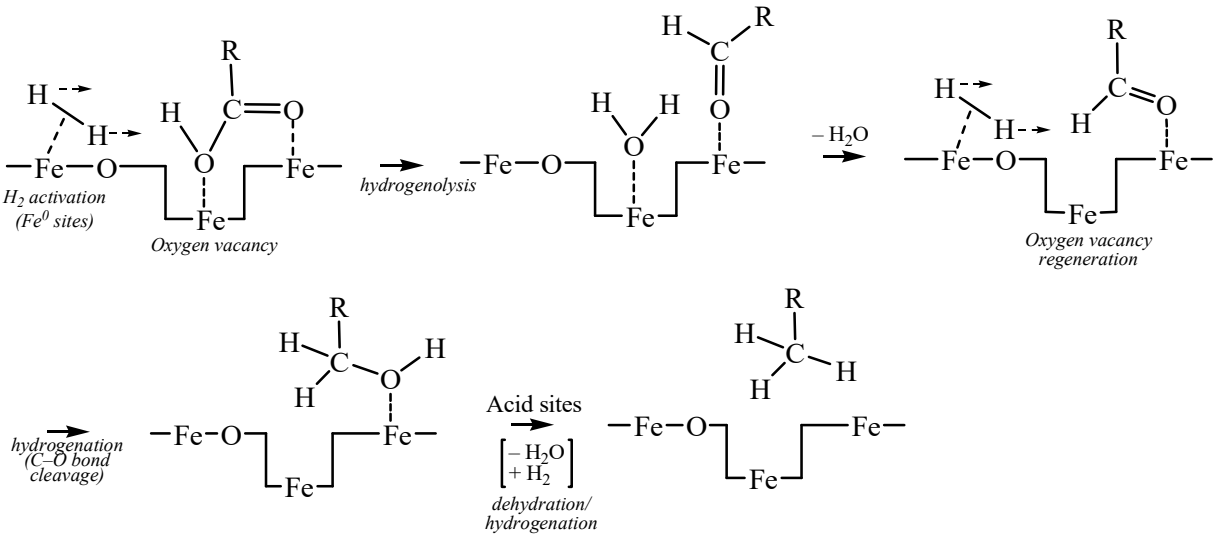
Due to the complex structure and the variable composition of the steel slag samples (Section 3.2), attempts were made to identify both the active species and a plausible mechanism operating in the HDO reactions under study. Regarding the active species, attention was paid to the iron oxide components ($FeO_x$), which are abundant in the slag matrix (21–32%, see Table 2) and have long been known to be HDO catalysts, specifically in the selective reduction of carboxylic acids to aldehydes [27,28]. Many different Fe-based catalysts have been studied in this field [29], for example in the hydrodeoxygenation of lignin-derived phenolic compounds [30] and in the deoxygenation of fatty acids [31,32]. However, very few HDO studies have focused on pure iron/iron oxide phases as bulk catalysts. On this basis, guided by the literature and appropriate experimental data, we formulated the following hypotheses on the role of the catalyst material.

#### 3.1.1. The Plausible Mechanism

Iron shows more promising features as an HDO catalyst candidate compared with other non-noble metals such as Ni and Co, as it is among the cheapest and most abundant transition metals [33]. In addition, due to its high oxygen affinity, it exhibits a higher oxygen removal percentage, a useful feature for the regeneration of oxygen vacancies, which is a crucial HDO pathway.

From a mechanistic point of view, it is well known that deoxygenation of carboxylic acids requires the coexistence on the catalyst surface of multiple functionalities, such as metallic sites to deliver hydrogen, acid sites for alcohol dehydration, and oxygen vacancies for C-O cleavage and oxygen abstraction [7]. The synergistic effect of these sites determines a partial or complete deoxygenation.

Recent studies on iron-based HDO catalysts [5,29,31] suggested the pathways depicted in Scheme 2.




**Scheme 2.** Plausible mechanism for HDO of fatty acids on slag catalyst.

At first, activated hydrogen at the metallic $Fe^0$ sites on the slag surface migrates (by spillover) to the fatty acid, which in turn is bound to oxygen vacancies, and this favors

multiple C-O bond scission, affording aldehyde and alcohol. Next, dehydration and hydrogenation reactions on acid sites lead to alkene and alkane formation.

The hypothesis of a mechanism based on the coexistence of different active sites is corroborated by recent studies [32], suggesting an active transformation of the catalyst surface through a continuous reduction by $H_2$ and oxidation by the carboxylic acid, presumably through a reverse Mars–van Krevelen mechanism [34].

The oxygen vacancies, created by hydrogen reduction, can abstract oxygen atoms from fatty acids, restoring the initial surface structure. Similar conclusions on the formation of a Fe(0) phase were reached by Pestman et al. in studies on the HDO of acetic acid to acetaldehyde over iron oxides [35]. Alternatively, water release after the first step could regenerate the vacancy, or oxygen could remain inside the oxide lattice, filling the vacancy itself.

Experimental proofs were sought to support these assumptions. Specifically, in-depth XRD analyses of slag samples (Table S1 and Figures 7, S1, S2 and S7) provided valuable information on the crystalline phases, showing that Fe(0) (metallic) weight percentage increases under the hydrogenation conditions, corroborating the hypothesis of an active transformation of the slag surface.

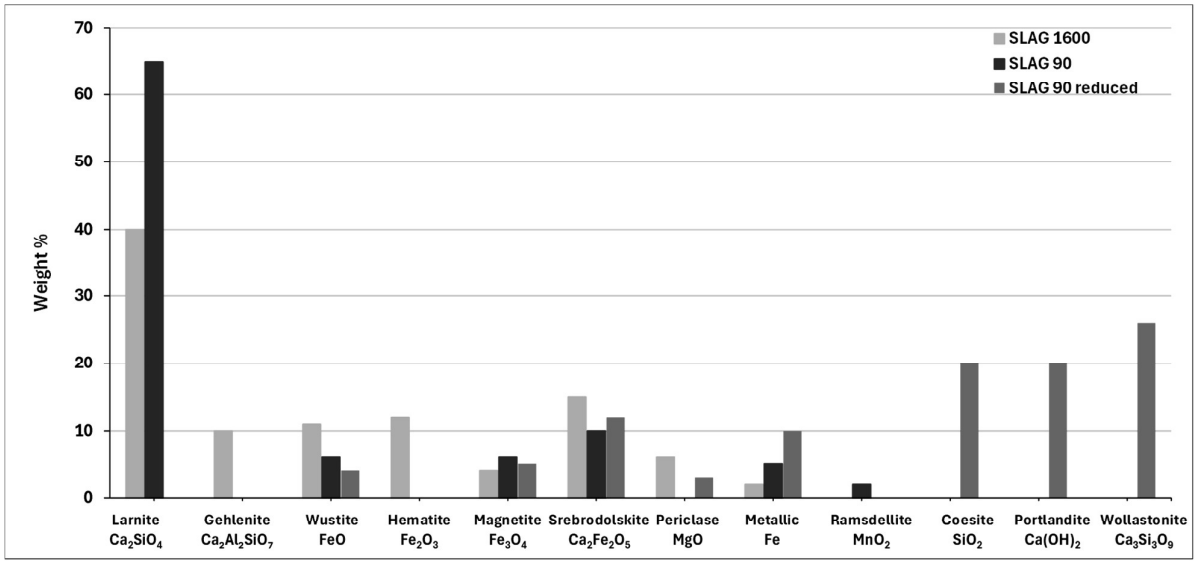
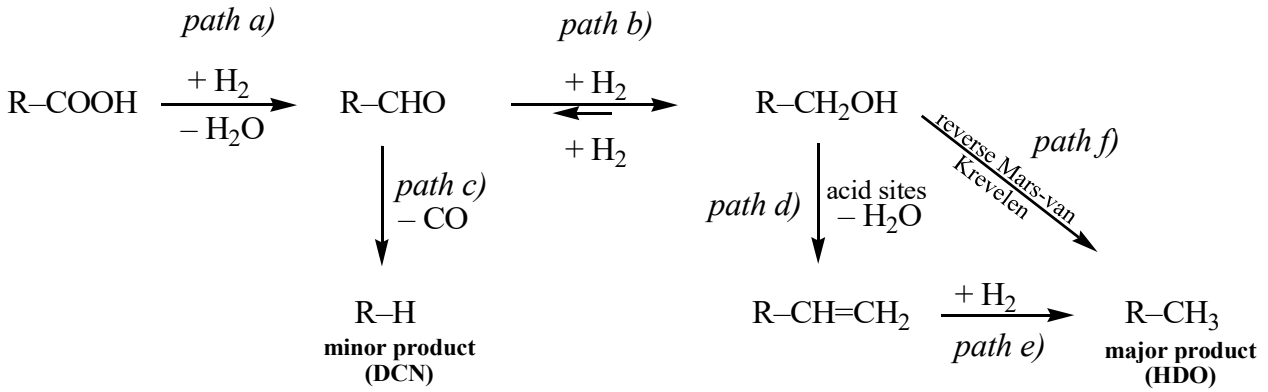



**Figure 7.** XRD analyses of slag fractions.

### 3.1.2. HDO vs. DCN Selectivity

Another crucial aspect addressed was explaining the high selectivity exhibited by the slag catalyst. The tendency of Fe to favor hydrodeoxygenation (HDO) over decarbonylation (DCN) can be directly related to the high iron oxyphilic nature and consequently to the strength of the Fe–O bonds formed during the reaction (see Scheme 2) [36]. This capacity allows for longer retention times of the oxygenated intermediates on the slag surface, preventing the reaction from stopping at the carbonyl stage (Scheme 3, path a), thus enabling the successive steps of alcohol formation (path b) and dehydration/hydrogenation (paths d–e) that afford the HDO product R-$CH_3$ [32]. An opposite selectivity is generally observed with Pd, Ni and Co metals, which display a carbophilic nature and tend to form weaker bonds with oxygen, thus stopping the reaction pathway at the carbonyl stage and consequently favoring the decarbonylation product R-H (path c) [11,37].

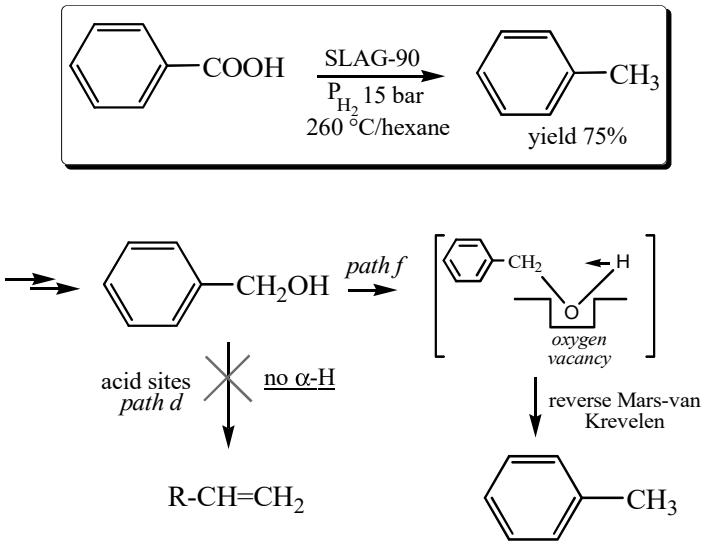



**Scheme 3.** Representative pathways for HDO versus DCN selectivity with slag catalyst.

Special attention was also paid to establishing the role played by the slag lattice in this process to understand if it takes part in drawing the selectivity toward hydrodeoxygenation products.

The ammonia-TPD profile (Figure 4b) showed SLAG-90 displaying a surface acidity of 100 μmol/$m^2$, with acid sites of both weak and medium strength. These data can explain the capacity of the catalyst to perform the final steps of alcohol dehydration/hydrogenation in Scheme 3 (path d–e), producing the HDO product. Remarkably, the slag also possesses basic sites, as shown by the $CO_2$-TPD profile (Figure 4a), that do not seem to hinder the HDO process, but, on the contrary, could favor it by improving the adsorption of fatty acid molecules on the slag surface through an acid-base reaction.

Nevertheless, another mechanism that is alternative to paths d–e, known as the reverse Mars−van Krevelen pathway (path f), is often invoked in the case of the HDO process over reducible metal oxides. In this route, the catalyst can directly remove the O atom from the alcohol by C−O bond scission over an oxygen vacancy with a simultaneous H back-donation from the OH, leaving the O in the oxide lattice [31,38]. To ascertain if this mechanism is operating with slag, a control experiment was carried out by submitting benzoic acid to HDO conditions [32]. The yield of 78% confirmed our assumption, as benzyl alcohol, one of the key intermediates, is forced to react via a reverse Mars−van Krevelen kind of mechanism rather than dehydration/hydrogenation because of the lack of α-H (Scheme 4).




**Scheme 4.** A reverse Mars-van Krevelen mechanism involved in the slag-catalyzed HDO of benzoic acid.

### *3.2. Recycling Experiments*

Recycling tests were conducted to evaluate the deactivation resistance of the slag catalyst under HDO conditions. Due to the large-volume availability of slag and its virtually zero cost, the potential industrial application of this material was verified using soybean oil as a model triglyceride representative of waste lipid feedstocks used in a real industrial process of biofuel production (WCO, exhaust and fish oils, etc.) (Table S2).

The results listed in Figure 8 clearly show that the steel slag catalyst exhibits good performance and stability across six recycling experiments, displaying no loss of catalytic efficiency without any regeneration treatment. This statement was also corroborated by ICP-MS analyses, resulting in a total iron content of 13.0% for the initial sample and 10.5% for the recycled one. The absence of deactivation, even when switching to a more complex substrate, underscores the inherent stability and promising potential for successful scale-up of this catalytic system to the industrial level.

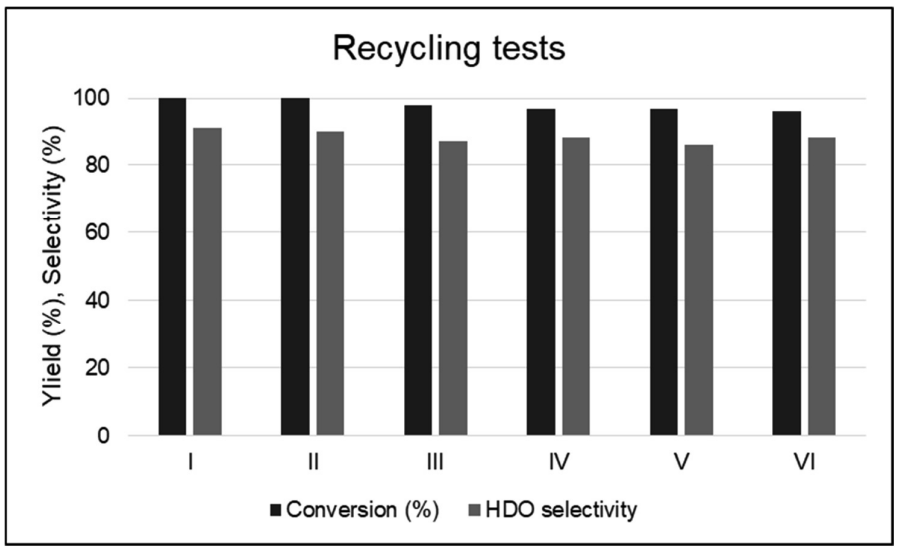



**Figure 8.** Recycling tests for HDO of soybean oil catalyzed by SLAG-90, Roman numerals are associated with the corresponding catalytic recycling test (for details see Section 2.3).

### *3.3. Comparison of Slag Catalytic Performance*

To highlight the qualities of slag as a catalytic material, its performance in the HDO process was compared with that of the most efficient Fe-based catalysts reported in the literature. Based on the data in Table 5, it clearly emerges that the slag is a superior HDO system. While it is active in the pristine form, the analogous catalysts require complex preparation procedures (commonly impregnation followed by calcination). In addition, slag can operate under milder temperatures and $H_2$ pressure conditions, enabling a more convenient and sustainable industrial process.

**Table 5.** Comparison with Fe-based catalysts for HDO reactions reported in the literature.

| Catalyst ($Co_{ntent}$ %) | Feedstock/Loading | HDO Conditions | Results | Ref. |
|---|---|---|---|---|
| BOF steel slag (20–25%) (pristine material, ground, no-chemical pretreatment) | Substrate = palmitic acid Sub/catalyst = 2:3 (*w*/*w*) | $P_{H2}$ 15 bar, 260 °C, 5–10 h solvent = heptane | Conv. >99% $HDO_{selectivity}$ 90% | This work |
| Fe-N-C@$Al_2O_3$ (20%) (complex procedure for catalyst preparation) | Substrate = stearic acid Sub/catalyst = 3:2 (*w*/*w*) | $P_{H2}$ 40 bar, 320 °C, 8 h solvent = dodecane | Conv. >99% $HDO_{selectivity}$ 90% | [32] |
| Fe-MSN (6%) (complex procedure for catalyst preparation) | Substrate = oleic acid Sub/catalyst = 1:4 (*w*/*w*) | $P_{H2}$ 30 bar, 290 °C, 6 h solvent = hexane | Conv. >99% $HDO_{selectivity}$ 83% | [31] |

In addition, the industrial application of slag as an HDO catalyst presented a strategic trade-off between kinetic intensity and process sustainability compared to commercial catalysts ($NiMo/\gamma-Al_2O_3$, $NiW/\gamma-Al_2O_3$, $CoMo/\gamma-Al_2O_3$). Commercial catalysts exhibited higher intrinsic activity and standardized selectivity. In contrast, slag required more rigorous experimental optimization to calibrate the feedstock load and residence time (as previously highlighted), ensuring a balance between conversion rates and complete deoxygenation. Slag demonstrated superior mechanical robustness and a high resistance to impurities (S, N, P) found in crude biomass, which typically "poison" expensive commercial alternatives. Its mineral matrix is ideal for continuous operation in tubular reactors without significant structural degradation. While commercial catalysts involve high production costs and mining footprints, slag is a zero-cost industrial by-product. Utilizing slag facilitates a circular economy model, significantly reducing operational costs (OPEX) and the overall carbon footprint of biofuel production.

## 4. Materials and Methods

Reagents and solvents were procured from Sigma-Aldrich and used as received. Steel slag was provided by "Acciaierie d'Italia (ADI, Taranto, Italy)", the Italian industry that produces steel through an integrated cycle. The catalytic material used in this work was the Basic Oxygen Furnace (BOF) slag, which is produced during the process of converting pig iron into steel (see Section 3.1). For catalytic evaluation and to ensure the reproducibility of the samples, the slag was sampled and prepared in the ADI laboratories through grinding procedures to obtain particle sizes smaller than 1600 μm. Subsequently, the obtained material was further sieved to obtain 90–210 μm particle sizes (the amount of material smaller than 90 μm was negligible). The two samples were labeled as SLAG-1600 and SLAG-90 and were used throughout all the experiments without further treatment. Multi-sample analyses revealed optimal reproducibility throughout different industrial batches, maintaining an uncertainty in composition of less than 5%.

The hydrogen source was generated through a H2 Generator Desk (MicroPROGEL. Padova, Italy) with an available flow rate of up to 1200 cc/min, outlet pressure of up to 16 bars and hydrogen purity > 99.99999%.

### *4.1. Material Characterization*

#### 4.1.1. Mineralogical Analyses

Spectroscopic characterization was carried out by XRD, XRF and FESEM-EDX techniques to ensure the mineralogic (phases) and the chemical (elements or oxides) composition of slag materials. Analyses were conducted on both the pristine BOF slag and the various fractions obtained by grinding and sieving.

#### 4.1.2. Physiochemical Analyses

Surface areas and pore size distributions were derived from N2 adsorption/desorption isotherms at 77 K (using a Micromeritics Tristar analyzer, Norcross USA Micromeritics). The BET equation [39] was used to calculate the surface area from the N2 adsorption isotherm, and the BJH method [40] was used to assess pore size distribution. Total pore volume was taken at P/P0 = 0.99.

Further instrument details are reported in the Supplementary Materials.

### *4.2. General Procedure for HDO Reaction*

Typically, a stainless-steel autoclave reactor (300 mL) was filled with feedstock (stearic, palmitic acid, or soybean oil) (0.5–1 g) and the slag catalyst (0.1–0.3 g), together with a magnetic stirrer, after which the solvent was added (10 mL of hexane, heptane, or

tetradecane). Then, the reactor was shut, purged three times with $H_2$ and charged at the hydrogen pressure of 15–30 bar. After that, it was heated for five to ten hours at temperatures in the range of 260–340 °C while being stirred at 300 rpm.

Upon completion, the reaction mixture was centrifuged, and the supernatant was analyzed by GC/MS (GC-MS Shimadzu instrument Milano, Italy) to determine product yields and substrate conversions. For every experiment, the rate reproducibility was better than 5%.

The work-up was the same for recycling testing, and following centrifugation, the catalyst was recovered and dried at 60 °C for a few hours to eliminate any leftover solvent traces. The catalyst was then moved to the autoclave once more for the subsequent reaction.

### *4.3. Product Analysis*

The fatty acid composition of soybean oil was determined by standard analyses (see Table S1 for details). Hydrodeoxygenation products were examined as follows: a total of 1 mL of the liquid phase sample was taken from the reactor, and 200 mL of silylating agent BSTFA (N,O-Bis(trimethylsilyl)trifluoroacetamide) was added in order to analyze fatty acid conversion by GC-MS. Silylation was carried out for one hour at 60 °C. Tetradecane was added as an internal reference for quantitative calculations. The samples were analyzed using a GC-MS Shimadzu instrument, as reported in detail in the Supplementary Materials.

## 5. Conclusions

The results of the present study have shown that BOF steel slag, one of the main wastes from the steel industry, displays promising catalytic performance for green diesel production by the hydrodeoxygenation of lipidic matrices (fatty acids and triglycerides). The unrecycled slag, classified as waste, is a large-volume material available at virtually no cost and does not require any pretreatment to work in HDO, other than a light grinding (to less than 200 μm) to make the material more homogeneous and increase its specific surface.

In addition to being effective in the pristine state, slag is surprisingly selective (>90%) toward the most desirable hydrodeoxygenation (HDO) pathway, while minimizing the parasitic processes of cracking, decarbonylation (DCN) and waxes production.

Fe oxides, which are abundant in the slag matrix (20–25%), are assumed to be the active species together with $Fe^0$, which is generated during the reaction. The oxyphilic nature of iron justifies the high HDO selectivity, and acid and basic sites seem to work in synergy with iron sites.

In addition to its catalytic efficiency, the use of steel slag significantly contributes to waste valorization, offering a sustainable solution to large-scale industrial waste management. By utilizing this abundant by-product, the process not only reduces the environmental footprint of steel production but also minimizes the reliance on costly and resource-intensive catalyst production.

Finally, the slag proved to be robust and resistant to deactivation, with the ability to be recycled many times and to work on more complex substrates such as soybean oil. High availability, no cost, selectivity and stability render the BOF slag a promising candidate for successful scale-up to the industrial level in green diesel production.

**Supplementary Materials:** The following supporting information can be downloaded at https://www.mdpi.com/article/10.3390/catal16030205/s1, Instrument analyses, Figure S1: XRD analyses of SLAG-1600, Figure S2: XRD analyses of SLAG-90, Figure S3: SEM-EDX analyses of SLAG-1600 with 100 μm magnification, Figure S4: SEM-EDX analyses of SLAG-1600 with 25 μm magnification, Figure S5: SEM-EDX analyses of SLAG-90 with 100 μm magnification, Figure S6: SEM-EDX analyses of SLAG-90 with 25 μm magnification, Figure S7: XRD analyses of SLAG-90 reduced, Table S1: XRD

analyses of slag fractions, Figure S8: XRD analyses of SLAG-90 post reaction, Table S2: Fatty acids composition of soybean oil [41].

**Author Contributions:** Conceptualization: S.S., E.G. and A.N., Data Curation: S.S., E.G., L.D. and A.N., Formal Analysis: S.S., E.G., T.C., Investigation: S.S., E.G., T.C. and G.G., Methodology: S.S., E.G. and R.A., Supervision: L.D. and A.N., Validation: S.S., E.G., T.C. and F.T., Writing—original draft: S.S. and A.N., Writing—review and editing: E.G., T.C., R.A., M.S., L.D. and A.N. All authors have read and agreed to the published version of the manuscript.

**Funding:** This research was partially financed by the PNRR Italian Environmental and Energetic Safety Ministry project "Permanent" [M2C2 3.5].

**Data Availability Statement:** All data are incorporated into this article and its online ESI material.

**Acknowledgments:** A special thanks to the R&D section of Acciaierie d'Italia, with particular regard to Annamaria Lapenna and Giuseppe Dilauro.

**Conflicts of Interest:** The authors declare no conflicts of interest.

## Abbreviations

The following abbreviations are used in this manuscript:

| | |
|---|---|
| SLAG-1600 | Steel slag with particle sizes smaller than 1600 μm |
| SLAG-90 | Steel slag fraction of 90–210 μm particle sizes |

## References

1. Testa, L.; Chiaramonti, D.; Prussi, M.; Bensaid, S. Challenges and opportunities of process modelling renewable advanced fuels. *Biomass Convers. Biorefinery* **2024**, *14*, 8153–8188. [CrossRef]
2. Centi, G. (Ed.) *Book of Abstract. 13th International Conference on Environmental Catalysis (ICEC 2025)*; European Research Institute of Catalysis: Brussels, Belgium, 2025.
3. Varma, P.; Otageri, J.; Kandasubramanian, B. Biodiesel from fats: Fatty acid feedstock as a circular economy solution. *Int. J. Green Energy* **2024**, *21*, 2530–2550. [CrossRef]
4. Ding, S.; Parlett, C.M.A.; Fan, X. Recent developments in multifunctional catalysts for fatty acid hydrodeoxygenation as a route towards biofuels. *Mol. Catal.* **2022**, *523*, 111492. [CrossRef]
5. Goh, B.H.H.; Chong, C.T.; Ong, H.C.; Milano, J.; Shamsuddin, A.H.; Lee, X.J.; Ng, J.-H. Strategies for fuel property enhancement for second-generation multi-feedstock biodiesel. *Fuel* **2022**, *315*, 123178. [CrossRef]
6. Casiello, M.; Savino, S.; Massaro, M.; Liotta, L.F.; Nicotra, G.; Pastore, C.; Fusco, C.; Monopoli, A.; D'Accolti, L.; Nacci, A.; et al. Multifunctional halloysite and hectorite catalysts for effective transformation of biomass to biodiesel. *Appl. Clay Sci.* **2023**, *242*, 107048. [CrossRef]
7. Lucantonio, S.; Di Giuliano, A.; Rossi, L.; Gallucci, K. Green Diesel Production via Deoxygenation Process: A Review. *Energies* **2023**, *16*, 844. [CrossRef]
8. Ding, S.; Fernandez Ainaga, D.L.; Hu, M.; Qiu, B.; Khalid, U.; D'Agostino, C.; Ou, X.; Spencer, B.; Zhong, X.; Peng, Y.; et al. Spatial segregation of catalytic sites within Pd doped H-ZSM-5 for fatty acid hydrodeoxygenation to alkanes. *Nat. Commun.* **2024**, *15*, 7718. [CrossRef]
9. Phan, D.-P.; Le, V.N.; Nguyen, T.H.; Kim, H.B.; Park, E.D.; Kim, J.; Lee, E.Y. Effect of amino-defective-MOF materials on the selective hydrodeoxygenation of fatty acid over Pt-based catalysts. *J. Catal.* **2021**, *400*, 283–293. [CrossRef]
10. Zhou, L.; Zhang, L.; Li, J.; Xiao, T.; Luo, P.; Su, X.; Cheng, H.; Zhao, F. Hydrodeoxygenation of biomass-derived fatty acids and esters to biofuels on RuRe/ZSM-5 catalysts: Synergistic effects of ReOx and Brønsted acid sites. *Fuel* **2024**, *369*, 131746. [CrossRef]
11. Savino, S.; Ghedini, E.; Aloia, A.L.; Monopoli, A.; Taddeo, F.; Castiglia, T.; Nacci, A.; Yakushkin, S.; Likozar, B.; Casiello, M.; et al. Palladium supported over carbon nanotubes catalytic system for green diesel production. *Carbon Trends* **2025**, *21*, 100576. [CrossRef]
12. Duan, J.; Chen, S.; Yao, Q.; Wu, K.; Luo, F.; Wang, D.; Liu, P.; Jiang, J.; Zheng, Z. Tailoring nickel precursors on red mud supports for catalytic hydrodeoxygenation of palmitic acid towards green diesel production. *Renew. Energy* **2025**, *241*, 122279. [CrossRef]
13. Qian, Z.; Wang, L.; Da, W.; Zhang, G.; Tian, Z.; Zou, Q.; Yang, Y.; Wei, M. Highly-efficient NiCo alloy catalysts towards hydrodeoxygenation of fatty acids to prepare alkanes. *Mol. Catal.* **2025**, *572*, 114754. [CrossRef]
14. Euroslag. Available online: https://www.euroslag.com (accessed on 17 October 2025).

15. Gómez-Goiri, A.; Gutierrez-Aguero, I.; Garcia-Estevez, D. Leveraging Blockchain Usage to Enhance Slag Exchange. *Appl. Sci.* **2024**, *14*, 6243. [CrossRef]
16. Jacob, L. Ladle Furnace Slag: Synthesis, Properties, and Applications. *ChemBioEng Rev.* **2024**, *11*, 60–78. [CrossRef]
17. Hamza, M.; Ayoub, M.; Shamsuddin, R.B.; Mukhtar, A.; Saqib, S.; Zahid, I.; Ameen, M.; Ullah, S.; Al-Sehemi, A.G.; Ibrahim, M. A review on the waste biomass derived catalysts for biodiesel production. *Environ. Technol. Innov.* **2021**, *21*, 101200. [CrossRef]
18. Fusco, C.; Casiello, M.; Pisani, P.; Monopoli, A.; Fanelli, F.; Oberhauser, W.; Attrotto, R.; Nacci, A.; D'Accolti, L. Steel slag as low-cost catalyst for artificial photosynthesis to convert $CO_2$ and water into hydrogen and methanol. *Sci. Rep.* **2022**, *12*, 11378. [CrossRef]
19. Savino, S.; Guglielmo, G.; Muolo, R.; Kamal, K.M.; Fanelli, F.; D'Amato, G.; Bollella, P.; Tricase, A.; Casiello, M.; Attrotto, R.; et al. Tunable copper based slag catalyst for energy vectors production. *Case Stud. Chem. Environ. Eng.* **2025**, *11*, 101050. [CrossRef]
20. Casiello, M.; Losito, O.; Aloia, A.; Caputo, D.; Fusco, C.; Attrotto, R.; Monopoli, A.; Nacci, A.; D'Accolti, L. Steel Slag as New Catalyst for the Synthesis of Fames from Soybean Oil. *Catalysts* **2021**, *11*, 619. [CrossRef]
21. Fan, C.; Wei, R.; Cheng, T.; Sun, R.; Zhang, H.; Long, H. The positive contributions of steel slag in reducing carbon dioxide emissions in the steel industry: Waste heat recovery, carbon sequestration, and resource utilization. *Chem. Eng. J.* **2024**, *498*, 155379. [CrossRef]
22. Liang, M.; Kang, W.; Xie, K. Comparison of reduction behavior of $Fe_2O_3$, ZnO and $ZnFe_2O_4$ by TPR technique. *J. Nat. Gas Chem.* **2009**, *18*, 110–113. [CrossRef]
23. Jozwiak, W.K.; Kaczmarek, E.; Maniecki, T.P.; Ignaczak, W.; Maniukiewicz, W. Reduction behavior of iron oxides in hydrogen and carbon monoxide atmospheres. *Appl. Catal. A Gen.* **2007**, *326*, 17–27. [CrossRef]
24. Zhang, H.; Ding, L.; Long, H.; Li, J.; Tan, W.; Ji, J.; Sun, J.; Tang, C.; Dong, L. Influence of $CeO_2$ loading on structure and catalytic activity for $NH_3$-SCR over $TiO_2$-supported $CeO_2$. *J. Rare Earths* **2020**, *38*, 883–890. [CrossRef]
25. Foraita, S.; Liu, Y.; Haller, G.L.; Baráth, E.; Zhao, C.; Lercher, J.A. Controlling Hydrodeoxygenation of Stearic Acid to n-Heptadecane and n-Octadecane by Adjusting the Chemical Properties of $Ni/SiO_2$–$ZrO_2$ Catalyst. *ChemCatChem* **2017**, *9*, 195–203. [CrossRef]
26. Muñoz-Arjona, A.; Ayala-Cortés, A.; Stasi, C.D.; Torres, D.; Pinilla, J.L.; Suelves, I. Catalytic hydrodeoxygenation of waste cooking oil into green diesel range hydrocarbons: From batch to continuous processing. *Chem. Eng. J.* **2025**, *503*, 158303. [CrossRef]
27. Kuriacose, J.C.; Jewur, S.S. Studies on the surface interaction of acetic acid on iron oxide. *J. Catal.* **1977**, *50*, 330–341. [CrossRef]
28. Grootendorst, E.J.; Pestman, R.; Koster, R.M.; Ponec, V. Selective Reduction of Acetic Acid to Acetaldehyde on Iron Oxides. *J. Catal.* **1994**, *148*, 261–269. [CrossRef]
29. Nunes, P.B.M.; Strapasson, G.B.; Báfero, G.B.; Zanchet, D. Exploring Iron Oxide Catalysts for Acetone Hydrodeoxygenation: Making Use of an Earth-Abundant Resource. *J Braz. Chem Soc* **2024**, *35*, e20240126. [CrossRef]
30. Hong, Y.; Hensley, A.; McEwen, J.-S.; Wang, Y. Perspective on Catalytic Hydrodeoxygenation of Biomass Pyrolysis Oils: Essential Roles of Fe-Based Catalysts. *Catal. Lett.* **2016**, *146*, 1621–1633. [CrossRef]
31. Kandel, K.; Anderegg, J.W.; Nelson, N.C.; Chaudhary, U.; Slowing, I.I. Supported iron nanoparticles for the hydrodeoxygenation of microalgal oil to green diesel. *J. Catal.* **2014**, *314*, 142–148. [CrossRef]
32. Li, J.; Zhang, J.; Wang, S.; Xu, G.; Wang, H.; Vlachos, D.G. Chemoselective Hydrodeoxygenation of Carboxylic Acids to Hydrocarbons over Nitrogen-Doped Carbon–Alumina Hybrid Supported Iron Catalysts. *ACS Catal.* **2019**, *9*, 1564–1577. [CrossRef]
33. McDonough, W.F.; Sun, S.S. The composition of the Earth. *Chem. Geol.* **1995**, *120*, 223–253. [CrossRef]
34. Mars, P.; van Krevelen, D.W. Oxidations carried out by means of vanadium oxide catalysts. *Chem. Eng. Sci.* **1954**, *3*, 41–59. [CrossRef]
35. Pestman, R.; Koster, R.M.; Boellaard, E.; van der Kraan, A.M.; Ponec, V. Identification of the Active Sites in the Selective Hydrogenation of Acetic Acid to Acetaldehyde on Iron Oxide Catalysts. *J. Catal.* **1998**, *174*, 142–152. [CrossRef]
36. Pestman, R.; Koster, R.M.; Pieterse, J.A.Z.; Ponec, V. Reactions of Carboxylic Acids on Oxides: 1. Selective Hydrogenation of Acetic Acid to Acetaldehyde. *J. Catal.* **1997**, *168*, 255–264. [CrossRef]
37. Peng, B.; Yuan, X.; Zhao, C.; Lercher, J.A. Stabilizing catalytic pathways via redundancy: Selective reduction of microalgae oil to alkanes. *J. Am. Chem. Soc.* **2012**, *134*, 9400–9405. [CrossRef]
38. Zacharopoulou, V.; Vasiliadou, E.S.; Lemonidou, A.A. Exploring the Reaction Pathways of Bioglycerol Hydrodeoxygenation to Propene over Molybdena-Based Catalysts. *ChemSusChem* **2018**, *11*, 264–275. [CrossRef]
39. Brunauer, S.; Emmett, P.H.; Teller, E. Adsorption of Gases in Multimolecular Layers. *J. Am. Chem. Soc.* **1938**, *60*, 309–319. [CrossRef]

40. Barrett, E.P.; Joyner, L.G.; Halenda, P.P. The Determination of Pore Volume and Area Distributions in Porous Substances. I. Computations from Nitrogen Isotherms. *J. Am. Chem. Soc.* **1951**, *73*, 373–380. [CrossRef]
41. Van Wijngaarden, D. Modified rapid preparation of fatty acid esters from lipids for gas chromatographic analysis. *Anal. Chem.* **1967**, *39*, 848–849. [CrossRef]

**Disclaimer/Publisher's Note:** The statements, opinions and data contained in all publications are solely those of the individual author(s) and contributor(s) and not of MDPI and/or the editor(s). MDPI and/or the editor(s) disclaim responsibility for any injury to people or property resulting from any ideas, methods, instructions or products referred to in the content.